Comparison between two different centrifugal acceleration directions for undercut slope modelling

Krit AROONWATTANASKUL[1*], Thirapong PIPATPONGSA[1]
Takafumi KITAOKA[1], Hiroyasu OHTSU[1]

[1] Graduate school of Engineering, Department of Urban management, Kyoto University
(Nishikyo-ku, Kyoto, 615-8540, Japan)
*E-mail: aroonwattanaskul.krit.23z@st.kyoto-u.ac.jp

Key Words : *undercut slope, centrifuge model, slope stability, radial gravity*

1. INTRODUCTION

The principles of centrifuge modelling are well understood now. Even though one of the major differences between a centrifuge model and the corresponding prototype is a radial centrifugal acceleration field, most theoretical and experimental analyses have not been taken into account for this difference. However, a better understanding of the centrifugal acceleration direction relative to the set-up of the model is necessary. This paper presents an investigation of the effect of the radial centrifugal acceleration field through the centrifuge model tests of undercut slope with two different slope directions, i.e., slope direction parallel to the axis of rotation and slope direction perpendicular to the axis of rotation. A series of experiments were conducted with a variation of undercut width; two experiments in a square container and two experiments in a rectangular container. The physical models were made of moist Edosaki sand with a set of miniature pressure cells embedded into the slope model. The centrifugal acceleration was gradually increased while monitoring the sequence of the collapse of the models. Finally, the behaviors before the onset of failure and mechanism of failure process in each slope direction were studied using image-based observation and stress distribution. The experimental centrifugal accelerations of the failures were compared to the theoretical idealization based on the arch failure assumption.

2. THEORETICAL BACKGROUND

Pipatpongsa et al. (2013) derived Eq. (1) to predict the maximum width of undercut slope under arch failure. The arching coefficient (k) is determined from a characteristic of each failure and theoretical mechanics, i.e. k=cos ϕ for strip arch with soil slip, k=1 for segmented arch with stable scarp and k=4/π for circular arch with abutment collapse.

$$B_f = \frac{k}{\left(\sin\alpha - \tan\phi_i \cos\alpha\right) - \left(c_i/\gamma T\right)} \frac{\sigma_c}{\gamma} \tag{1}$$

where B_f is the maximum stable width of sand block, α is the inclined angle, T is the thickness of soil block, ϕ_i is the interface friction angle, c_i is the apparent adhesion, σ_c is the unconfined compressive strength, γ is the bulk unit weight, ϕ is the internal friction angle of material used to build a slope.

3. METHODOLOGY

The centrifuge at the Disaster Prevention Research Institute, Kyoto University (DPRI-KU) was employed in this study. This beam centrifuge has a working radius of 2.5 m and a maximum acceleration of 200g. In this study, the maximum centrifugal acceleration was determined to be 50g. The tests were conducted with two different slope directions in each type of soil container (a square container and a rectangular container), i.e., slope direction parallel to the axis of rotation (Fig.1(a)) and slope direction perpendicular to the axis of rotation (Fig.1(b)).

(1) Square container

The physical models were made of moist Edosaki sand and constructed inside a 40 × 40 × 30 cm^3 aluminum container. Basic properties of Edosaki sand used in a square container are shown in Table 1. The model was divided into two parts as shown in Fig.2, basal support and slope part. Moist sand with an optimum water content of w=15.1% was compacted inside the model container to achieve a bulk density of ρ =1860 kg/m^3. The 40 cm wide, 15 cm long and 5 cm thick basal support was placed on a rigid plane covered by a sandpaper while the 40 cm wide, 25 cm long, 5 cm thick slope part was inclined by angle 40°on a rigid plane covered by a Teflon sheet for simulating the low friction interface plane. Pressure gauges were installed in the slope part during the compaction as outlined in Fig.3.

Table 1 Basic properties of Edosaki sand in a square container

Opitimum water content (w_{opt})	15.1 %
Maximum dry density ($\rho_{d\,max}$)	1700 kg/m^3
Unconfined compressive strength (σ_c)	5.7 kN/m^2
Interface friction angle (ϕ_i)	14.7 °
Apparent adhesion (c_i)	0.2 kN/m^2
Degree of compaction (D_c)	95 %

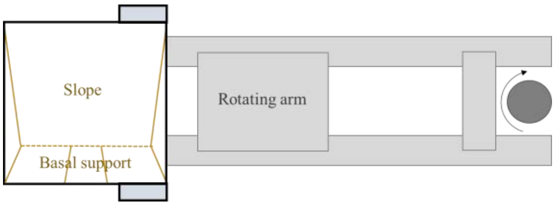

a) slope direction parallel to the axis of rotation

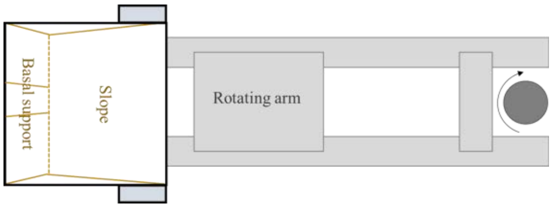

b) slope direction perpendicular to the axis of rotation

Fig. 1 Slope directions

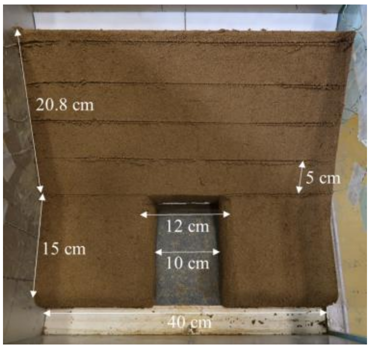

Fig.2 Physical model of an undercut slope in a square container

After preparation of basal support and slope part, the trapezoidal trench was excavated through the basal support to have a base width of 10 cm and a top width of 12 cm. Then, the marking lines were drawn on the surface every 5 cm from the bottom of the slope part for clear observation. A high-speed VDO camera was installed above the model to observe the movements of an undercut slope. To investigate the soil upheaval at basal support, 2 laser sensors were installed above and perpendicular to both sides of the pillars. Moreover, another laser sensor was installed at 4 cm from the bottom of the slope part to monitor the time when the failure occurred. The structure of the instrument is shown schematically in Fig. 3. The excavation was conducted in three steps at an average undercut width 11 cm, 16 cm, and 26 cm. The centrifugal acceleration was gradually increased until 50g at each step of excavation while monitoring the initial collapse of the models. After every step of the excavation, the centrifuge was stopped to dump the detached soil into the provided space in front of the model for preventing to be a bracer. A similar preparing procedure was repeated in a different slope direction.

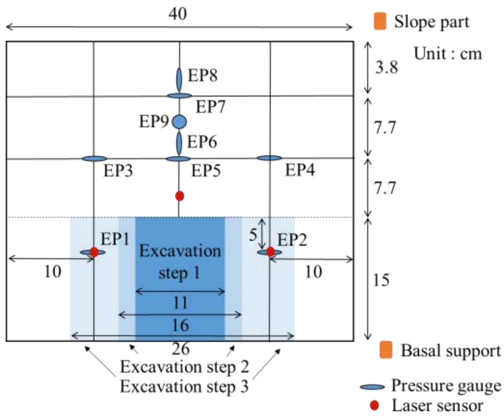

Fig. 3 The instrumented undercut slope model (perpendicular view to basal support)

(2) Rectangular container

The physical models were constructed inside a 63 × 20 × 30 cm^3 aluminum container, in which the longer side of the container is placed tangential to the axis of rotation. The physical models of two cases, narrow side slope model and wide side slope model were made of Edosaki sand. The models were compacted to the bulk density 1560 kg/m^3 and water content 10%. The schematic illustrations of the model slopes are shown in Fig. 4(a) as a narrow side slope model, Fig. 4(b) as a wide side slope model and Fig. 4(c) as a side view of slope models. Dimensions of the physical model and Edosaki sand properties used in a rectangular container are listed in Table 2. Pressure gauges were installed as outlined in Fig. 5(a) for a narrow side slope model and Fig. 5(b) for a wide side slope model. The trapezoidal trench was excavated like in a square container at an average undercut width 11 cm. Finally, the marking lines were drawn on the surface every 4 cm from the bottom of the slope part. During the test, the centrifugal acceleration was gradually increased while monitoring the initial collapse of the models. The tests were terminated when the centrifugal acceleration reached 50g.

Table 2 Basic parameters of model slopes in a rectangular container (* material properties from Khosravi et al. (2016))

Scale of model		Narrow side slope	Wide side slope
Dimensions	Slope width (cm)	20	63
	Slope length (cm)	15	15
	Slope thickness (cm)	5	5
	Slope angle (degree)	40	40
	Pillar width (cm)	5	26.5
	Pillar length (cm)	5	5
	Pillar thickness (cm)	5	5
Material properties (Edosaki sand)	Water content (%)	10	10
	Bulk unit weight (kN/m^3)	15.3	15.3
	Unconfined compressive strength (kN/m^2)	14.7*	14.7*
	Interface friction angle (°)	17.5 *	17.5 *
	Apparent adhesion (kN/m^2)	0*	0*
	Internal friction angle (°)	40.9	40.9

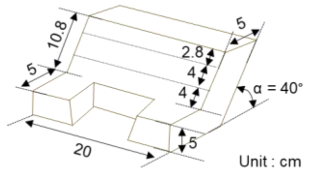

a) Narrow side slope model

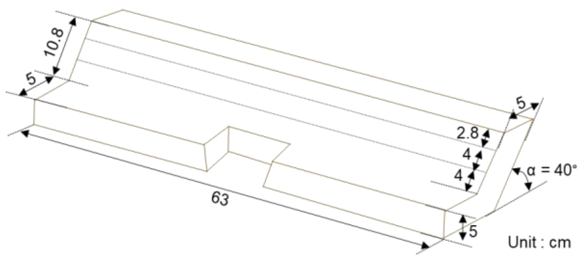

b) Wide side slope model

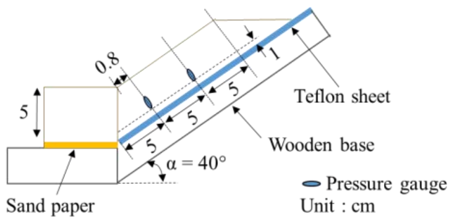

c) Side view

Fig.4 Outline of slope models in a rectangular container

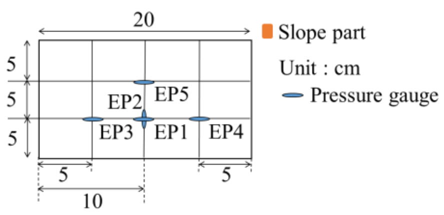

a) Narrow side slope model

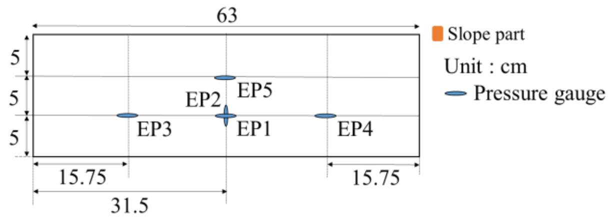

b) Wide side slope model

Fig.5 Location of pressure gauges (perpendicular view to slope)

4. RESULTS AND DISCUSSIONS

(1) Centrifugal acceleration

Table 3 Results of theoretical and experimental centrifugal acceleration in a square container

Average undercut width	Theoretical centrifugal acceleration	Experimental centrifugal acceleration (slope direction parallel to the axis of rotation)	Experimental centrifugal acceleration (slope direction perpendicular to the axis of rotation)
11 cm	12.8g	33.8g	27.9g
16 cm	8.8g	26g	21.7g
26 cm	5.4g	20.1g	14g

Table 3 shows the theoretical and experimental results of centrifugal acceleration in a square container. Substituting the material parameters in Table 1 into Eq. (1), B_f = 1.41 m on the prototype scale. This is equal to 12.8g, 8.8g and 5.4g in the centrifuge model for the average maximum stable width of sand block 11 cm, 16 cm, and 26 cm, respectively. However, for each of which, the failure of the slope direction parallel to the axis of rotation model was observed when the centrifugal acceleration reached 33.8g, 26g, and 20.1g while the failure of the slope direction perpendicular to the axis of rotation model occurred when the centrifugal acceleration reached 27.9g, 21.7g, and 14g. The centrifugal accelerations in both directions were higher than those predicted by the arch failure assumption. The derived equations show a good agreement with the experiments by giving the lower bound of theoretical centrifugal acceleration. Therefore, the derived equations are in the safe side design criteria.

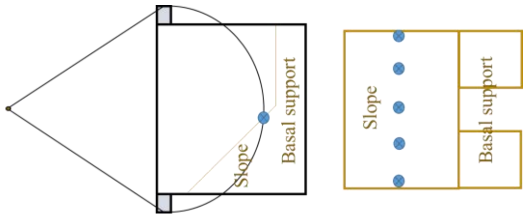

a) slope direction parallel to the axis of rotation

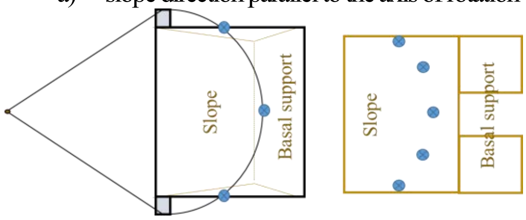

b) slope direction perpendicular to the axis of rotation
Fig. 6 Radial centrifugal acceleration field

After rotating the centrifuge, the container moved upward 90 degrees. The centrifugal acceleration field is constant at the same cross-section for slope direction parallel to the axis of rotation model (Fig. 6(a)). Whereas, the centrifugal acceleration field for slope direction perpendicular to the axis of rotation model is not constant and increases along to either edge of the centrifuge model (Fig. 6(b)). Therefore, the surplus load is increased by the radial centrifugal acceleration field resulting in earlier failure occurred. The error due to the radial centrifugal acceleration field is ~ 0.8 percent. It is a very small percentage. In a way, this may not affect the results much. The quantification and parameter descriptions of error due to the radial centrifugal acceleration field are described in detail by Madabhushi G. (2014). To minimize the above error is by choosing the suitable diameter of the centrifuge and making the centrifuge model curved. The larger the diameter of the centrifuge, the smaller this error appears. However, the influence of the centrifugal acceleration, the radius of the centrifuge, and the size of a model container vary from problem to problem and from parameter to parameter measured (Zeng X. and Lim S. L. (2002)).

Table 4 Results of theoretical and experimental centrifugal acceleration in a rectangular container

Model type	Theoretical centrifugal acceleration	Experimental centrifugal acceleration
Narrow side slope model	21.7g	31.6g
Wide side slope model	21.7g	22.5g

Table 4 shows the theoretical and experimental results of centrifugal acceleration in a rectangular container. By substituting the parameters from Table 2 into Eq. (1), B_f solved by average maximum stable width of sand block 11 cm is equal to 21.7g. The failure was observed in a narrow side slope model when the centrifugal acceleration reached 31.6g. Nevertheless, the failure was observed at 22.5g in a wide side slope model. The centrifugal acceleration in a narrow side slope model was higher than that of a wide side slope model because a portion of the load above the trench transfers toward the side-supporting rigid plates, resulting in higher stability of the slope. (Aroonwattanaskul K. and Pipatpongsa T. (2019)).

(2) Modes of failure

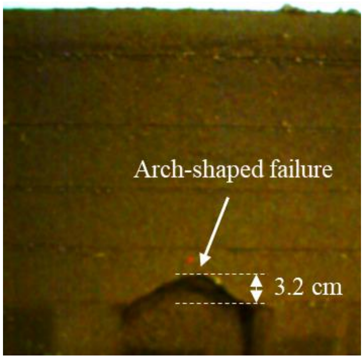

a) Undercut width 11 cm

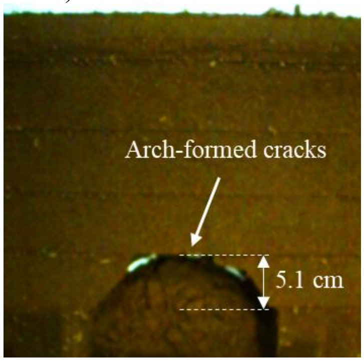

b) Undercut width 16 cm

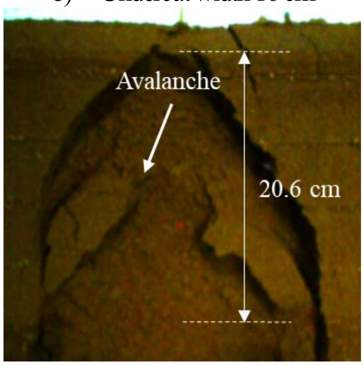

c) Undercut width 26 cm
Fig. 7 Sequence of failure for slope direction parallel to the axis of rotation

Photos of the failure in a square container captured by a high-speed VDO camera for slope direction perpendicular to the axis of rotation and slope direction parallel to the axis of rotation are shown in Fig. 7 and 8, respectively. During step 1 of the excavation, with a span of 11 cm, an initial arch-shaped failure occurred in front of the slope above the undercut part (Fig. 7(a)). While increasing centrifugal acceleration until 50g, the undercut slope remained a stable scarp on the slope after an initial arch failure. The excavation span increased to 16 cm during step 2. With this span, the slope failed with a continuous sequence of arch-formed cracks until reaching the excavated width (Fig. 7(b)). Expanding the excavation span to 26 cm in step 3 resulted in an avalanche of the center part of the slope until the top edge of the slope (Fig. 7(c)). The test for slope direction parallel to the axis of rotation model showed a similar sequence of failure as shown in Fig. 8(a) to 8(c).

The failure mode for a narrow side slope model in a rectangular container started with spalling on both sides of basal support and led to local failure along the edge of the scarp above the excavated part. While increasing centrifugal acceleration until 50g, the undercut slope remained a stable scarp on the slope after progressive local failures as shown in Fig. 9(a). The first failure in a wide side slope model occurred in an arch-shaped failure due to less effect from the side boundaries. Then, the slope failed with a continuous sequence of arch-formed cracks and started to fail at the corner of the pit due to the maximum stress concentration. Finally, the failure process stopped with a stable scarp above the arch-formed failed area and basal support collapsed as shown in Fig. 9(b).

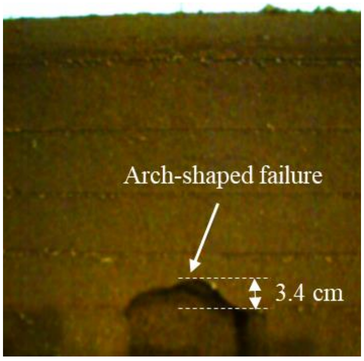

a) Undercut width 11 cm

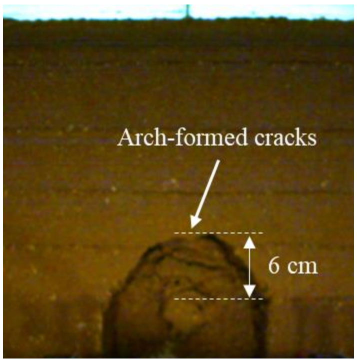

b) Undercut width 16 cm

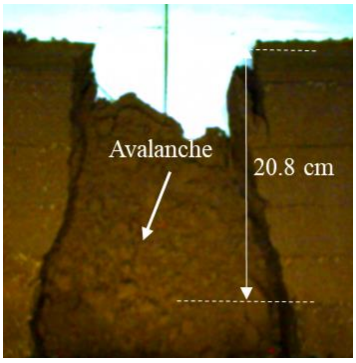

c) Undercut width 26 cm

Fig. 8 Sequence of failure for slope direction perpendicular to the axis of rotation

a) Narrow side slope model

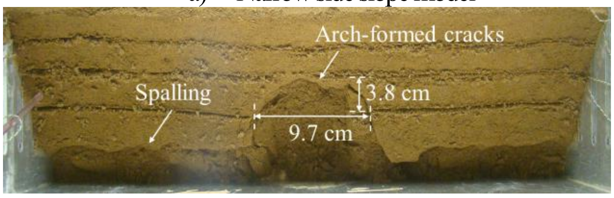

b) Wide side slope model

Fig. 9 Modes of failure

(3) Stress distribution

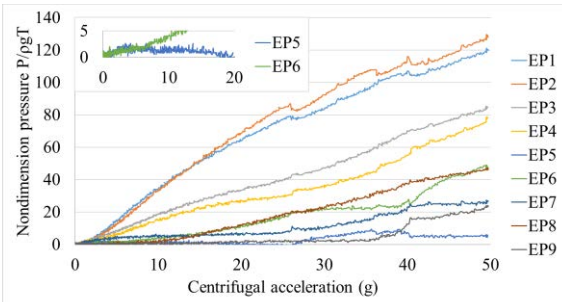

a) slope direction parallel to the axis of rotation

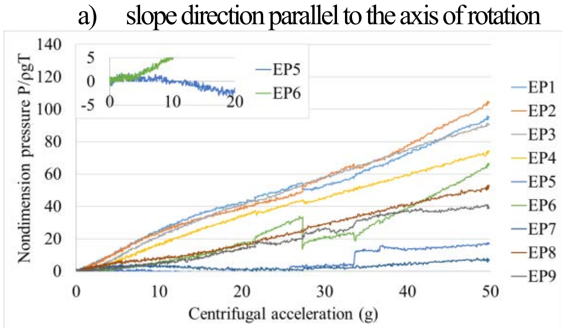

b) slope direction perpendicular to the axis of rotation

Fig. 10 Changes of earth pressure at undercut width 16 cm

During the centrifuge test, the pressure gauges were monitored and recorded. These data were normalized by ρgT and plotted with centrifugal acceleration in Fig.10 for the tests in a square container at an average undercut width 16 cm. Where ρ is the bulk density of sand, g is the gravitational acceleration and T is the thickness of a soil block. By increasing the centrifugal acceleration, each pressure gauge starts to increase the pressure. Earth pressures in the pillars (EP1 and EP2) steadily increased until the first failure of the model occurred. The laser sensors at both sides of the pillars represent almost no change in level during the experiment indicating no upheaval at the basal support. The pressures on two sides of the slope model (EP3 and EP4) increased gradually by the load transfer from the central body of the slope to the adjacent stationary sides. While the pressure at the center of the slope along the dip direction (EP5) decreased, the pressure along the transverse direction (EP6) increased in both models as shown in Fig. 10(a) and 10(b). The results confirm the development of passive arch action before the arch-shaped failure as reported by Khosravi et al. (2011).

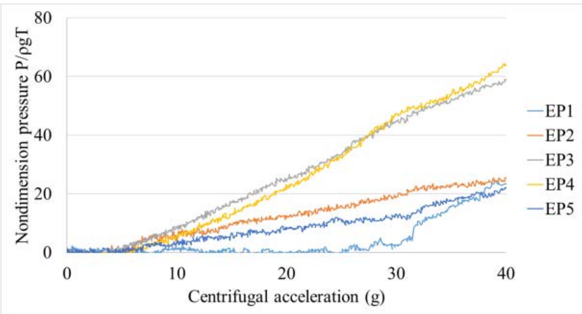

a) Narrow side slope model

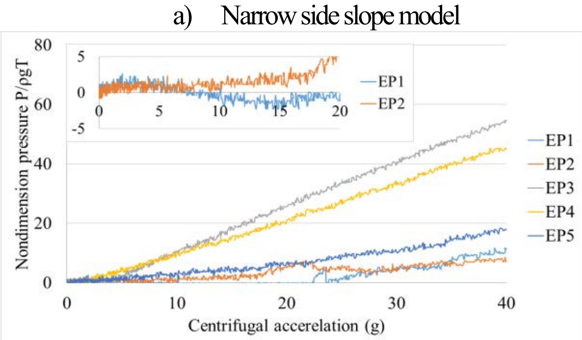

b) Wide side slope model

Fig. 11 Changes of earth pressure in a rectangular container

Nondimension pressures were plotted with centrifugal acceleration in Fig.11(a) and 11(b) for a narrow side slope model and a wide side slope model. Only EP1 in a narrow side slope model showed a little change after the local failure occurred. While the pressures in a wide side slope model were consistent with the arching effect when the load transfers from the yielding central part to the adjacent stationary parts of the model.

5. CONCLUSIONS

The effect of the radial centrifugal acceleration field was investigated by comparing the behaviors of the centrifuge model tests of undercut slope with two different slope directions and two different sizes of soil container. This study revealed that the set-up of the model by slope direction parallel to the axis of rotation is more practical and suitable than slope direction perpendicular to the axis of rotation due to the constant centrifugal acceleration at the same cross-section. However, the failure mechanism of both directions in a square container can still be reliably demonstrated by showing a similar sequence of failure. On the other hand, the interruption of side boundaries can change the mode of failure from arch-shaped failure to local failure along the edge of scarp.

Although the error due to the radial centrifugal acceleration field is a small percentage, it can have a significant impact on physical models and sensors. Therefore, the variation in centrifugal acceleration and the side boundaries imposed by model containers should be properly taken into account.

ACKNOWLEDGEMENT

This research was supported by Japan International Cooperation Agency (JICA)

REFERENCES

1) Pipatpongsa, T., Khosravi, M. H. and Takemura, J.: Physical modeling of arch action in undercut slopes with actual engineering practice to Mae Moh open-pit mine of Thailand, ICSMGE18, pp. 943-946, 2013.

2) Khosravi, M. H., Pipatpongsa, T., Takahashi, A., and Takemura, J.: Arch action over an excavated pit on a stable scarp investigated by physical model tests, Soils Found, 51(4), pp. 723–735, 2011.

3) Khosravi, M. H., Takemura, J., Pipatpongsa, T. and Amini, M.: In-flight excavation of slopes with potential failure planes, Journal of Geotechnical and Geoenvironmental Engineering, 142(5), 06016001, 2016.

4) Madabhushi G.: Centrifuge modelling for civil engineers. Boca Raton, London, New York: CRC Press. Taylor & Francis Group, p. 292, 2014.

5) Zeng, X. and Lim, S. L.: The Influence of Variation of Centrifugal Acceleration and Model Container Size on Accuracy of Centrifuge Test, Geotechnical Testing Journal, GTJODJ Vol. 25, No. 1, pp. 24–43, March 2002.

6) Aroonwattanaskul, K. and Pipatpongsa T.: Effect of side boundaries on an undercut slope studied by centrifuge models, Proceedings of the 40th West Japan symposium on Rock Engineering, pp. 41-44, 2019.